Improving fast pyrolysis of lignin using three additives with different modes of action

Ghysels, Stef; Dubuisson, Ben; Pala, Mehmet; Rohrbach, Leon; Van den Bulcke, Jan; Heeres, Hero Jan; Ronsse, Frederik

Published in:
Green Chemistry

DOI:
10.1039/d0gc02417a

Publication date:
2020

Green Chemistry

PAPER

View Article Online
View Journal | View Issue

Cite this: *Green Chem.*, 2020, **22**, 6471

Improving fast pyrolysis of lignin using three additives with different modes of action†

Stef Ghysels, *[a] Ben Dubuisson,[a] Mehmet Pala,[a] Léon Rohrbach,[b] Jan Van den Bulcke,[c] Hero Jan Heeres[b] and Frederik Ronsse[a]

Received 15th July 2020,
Accepted 20th August 2020

DOI: 10.1039/d0gc02417a

rsc.li/greenchem

Lignin holds the potential to obtain key monoaromatic compounds upon its depolymerization. Depolymerization of woody biomass by pyrolysis is well established but often unsuccessful for lignin due to a combination of its melting, agglomeration, and modest yields towards aromatics. Therefore, several lignin additives have been put forth to overcome one or more of these hurdles. Although some seem promising, a direct comparison is obscured by differences in applied technical lignin types, reactor configurations/scales, and product analyses. Moreover, the effects of additives have either been evaluated mostly on an analytical scale or their mode of action is not entirely understood. This work involves the addition of clays, calcium hydroxide and sodium formate to lignin, each having a different (putative) mode of action, in a well-defined and comparable manner. Organosolv lignin and lignin with additives were analysed by TGA/DSC and py-GC/MS. Pyrolysis was performed in a lab-scale reactor (350 g feeding). The pyrolysis liquids were characterised through elemental analysis, GCxGC-FID, GCxGC-HR-ToF-MS, GPC, and HSQC NMR analyses. All additives overcame melting issues and led to increased liquid yields but the most promising were attapulgite and calcium hydroxide. Lignin with attapulgite resulted in a heavy phase with the highest carbon yield (25.7%) and a substantial monomer yield (18.9%, mostly alkylphenols). Lignin with calcium hydroxide resulted in a heavy phase with the highest monomer yield (23.8%, mostly alkylphenols) at a substantial carbon yield (15.1%). The pyrolysis mechanisms for lignins with additives are elaborated and updated in this work.

1. Introduction

Lignin is the most abundant biopolymer on Earth, after cellulose.[1,2] Yet, there exists a certain discrepancy between the high valorization potential of lignin and its currently underexploited use in biorefinery schemes. Research on lignin valorization can generally be classified into three groups, based on process-induced changes in the degree of polymerization. Carbon fibres from the (co-)spinning of lignin,[3,4] hierarchically porous carbons[5,6] and biochar[7] are examples that follow from thermal carbonization and cross-linking, giving these materials a high degree of polymerization/aromatization, making them suitable for applications as electrode material for supercapacitors, soil amendment, among others. Examples of products in which the polymeric properties are retained[8] are *e.g.*, additives for rubber,[9] epoxy resins,[10] UV blocking films[11] and asphalt.[12] The vast majority of research, however, focuses on lignin depolymerization, as well as post-processing and applications of (aromatic) depolymerization products for chemicals or fuel.[13–18]

Among the options for lignin depolymerization are reductive and oxidative depolymerization, acid- or base-catalyzed depolymerization, solvolytic depolymerization, and thermal depolymerization through, for instance, fast pyrolysis.[16] Among these, fast pyrolysis is principally the most simple conversion process due to the absence of applied pressure, solvent or, in plain fast pyrolysis, a catalyst. In fast pyrolysis, biomass is rapidly heated to *ca.* 500 °C in the absence of oxygen. Upon quick quenching of pyrolysis vapors, pyrolysis liquids are obtained in yields that amount to 75 wt% for lignocellulosic biomass,[19] while typically ranging from 10 to 40 wt% for lignin.[20] It is these pyrolysis liquids that contain the mono-aromatic compounds of interest.

A vast number of studies on the fast pyrolysis of lignin concern analytical pyrolysis.[21–24] However, results from analytical pyrolysis cannot be directly translated to what is expected

[a]*Thermochemical Conversion of Biomass Research Group, Department of Green Chemistry and Technology, Ghent University, Coupure Links 653, 9000 Ghent, Belgium. E-mail: Stef.Ghysels@UGent.be*
[b]*Department of Chemical Engineering (ENTEG), University of Groningen, Nijenborgh 4, 9747 AG Groningen, The Netherlands*
[c]*Laboratory of Wood Technology (UGent-Woodlab), Department of Environment, Ghent University, Coupure Links 653, 9000 Ghent, Belgium*

†Electronic supplementary information (ESI) available. See DOI: 10.1039/D0GC02417A

from larger scale pyrolysis units, given the longer hot-vapor residence time and vapor condensation present in the latter.[25] Up-scaling from analytical pyrolysis to large-scale pyrolysis of lignocellulosic biomass has been proved on a large scale.[26] Yet, pyrolyzing isolated lignin with the same reactor technology usually is not successful;[27] it is often impossible to run fast pyrolysis experiments in lab-scale reactors for several hours. The reason for this is three-fold. First, technical lignins are found to be very sticky and dusty powders. As a result, plugging and clogging of auger and lock-hopper feeding systems often occurs.[27–29] Next, the tendency of technical lignins to soften, with the formation of a rubbery substance and melting at pre-pyrolysis temperatures is a concern.[30] The sticky melt forms agglomerates (with bed material such as sand) and ultimately causes blockages inside the pyrolysis reactor.[31–33] Finally, in early stages of lignin pyrolysis, radical intermediates are formed,[24,34–36] which undergo repolymerization, leading to the formation of larger molecular-weight compounds and solid char.[37,38]

To facilitate lignin feeding, reactors were modified[28] and[29] slug injection was performed by pneumatic transport. To boost the yield of liquid products with low molecular weight, hydropyrolysis has been proposed. In hydropyrolysis, hydrogen gas and an appropriate catalyst are used to generate hydrogen radicals to quench lignin-derived radical intermediates, and by doing so, prevent repolymerization.[39–41] However, hydropyrolysis is performed at an increased pressure with catalysts, while the primary (hydro)pyrolysis products, being mono-aromatic compounds, may be overhydrogenated to cycloalkanes.[42–44]

To improve lignin pyrolysis and minimize modifications to pyrolysis reactors for whole biomass, specific additives can be applied to either facilitate feeding, prevent melting, prevent bed agglomeration or improve liquid yield. Three additives were selected for further analysis because of a combination of the following reasons: (i) all three lignin additives have been described in patent literature (industrial relevance) and shown to enhance lignin pyrolysis (ii) pyrolysis of lignin with (one of) the additives is largely dominated by analytical pyrolysis; and (iii) the mode of action of (one of) the additives is not fully elucidated.

The first additive to lignin constitutes various clays. An equal lignin/clay ratio was applied Ref. 45, while Ref. 46 mixed clay with lignin to obtain a mixture with 30 wt% clay and 70 wt% lignin. The positive effect of clay has been ascribed to the dilution of lignin, which becomes less prone to melting. The lignin/clay mixture also produces more rigid particles upon pelletization that have improved feeding characteristics.[45,46] The second additives to lignin comprise formate salts for *in situ* hydrogen production at atmospheric pressure to quench radical quinone methide intermediates.[47–49] The application of formate salts was first described by Ref. 49. From that point, follow-up studies entirely concerned analytical pyrolysis, applying different formate salts and deuterated formate.[47,48,50,51] Reactor-scale pyrolysis has thus been underexplored. The third additive was calcium hydroxide to reach 5 wt% calcium hydroxide in the prepared lignin.[52] The putative mode of action is ascribed to calcium hydroxide that chemically binds with specific lignin functional groups, but the exact working mechanism is not entirely understood nor elaborated, despite various follow-up studies.[51,53,54] In addition, various doses of calcium hydroxide have been applied. While Ref. 49 included a calcium hydroxide treatment (20 wt%) to benchmark calcium formate,[51] applied calcium hydroxide at 9.3 wt% and[54] at 5 wt%. Direct cross-comparison of all three additives is also obscured by the differences in the type of lignin, reactor configuration/scale, and product analyses.

This work therefore evaluates these three distinct additives for one type of lignin, using one reactor type, and one set of analytical tools. The objective of this study was two-fold: (i) to identify the additives that facilitate reactor feeding for fast pyrolysis and that result in the highest yield of monoaromatic compounds; and (ii) to elucidate and revise the working mechanism of pyrolysis of the lignins with additives. To that end, results were compared on a technical level (feeding, melting, *etc.*) as well as on a chemical level (product yields, liquid's composition, *etc.*). Organosolv lignin was selected as the starting material for this study as this lignin is most similar to native *in planta* lignin,[13,15] in contrast to *e.g.*, Kraft lignin or lignosulfonates.

This work is conceived as follows. First, results from all experiments and analyses are presented to mutually compare the different additives. Then follows a dedicated section where various observations of pyrolysis of lignin with a certain additive are highlighted and merged to refine and update the pyrolysis mechanisms on the molecular level of the lignins with additives.

2. Experimentation

2.1. Organosolv lignin

Organosolv lignin (97.55 wt% dry matter) was kindly provided by Fraunhofer-Gesellschaft from Germany. A detailed description of Fraunhofer's organosolv process is described by Ref. 55 and summarized in ESI.† Fig. 1 in ESI† presents a magnified image of the as-received powdery organosolv lignin. The organosolv lignin was suspended in water, filtered, and the filter cake was dried to obtain particles of size 2–4 mm for lab-scale pyrolysis because the as-received lignin powder was unpractical to manipulate and because the application of additives involved a suspension step as well. Specifically, the as-received lignin was intensively mixed with water in a 10 L Scott bottle to make a slurry, which was passed over a vacuum Buchner filter with filter paper (grade 589/1, 12–25 μm). The solids on the filter paper were subsequently dried at 75 °C to form a solid, hard filter cake.

2.2. Preparation of lignin with additives

2.2.1. Addition of clay. Three types of natural clay were added to the organosolv lignin, attapulgite, bentonite and sepiolite (all are palygorskite-types of clays, *i.e.* magnesium aluminium phyllosilicates). These clays were kindly provided

by the Tolsa Group (Spain) under their commercial names: Cimsil G30 (attapulgite), Pangel M280 (bentonite), and Pangel S9 (sepiolite).

As the TGA/DSC and py-GC/MS analyses showed only minor differences among the three lignin/clay mixtures (*vide infra*), attapulgite was arbitrarily selected for lab-scale pyrolysis. Hence, one kilogram of attapulgite and one kilogram of as-received organosolv lignin were weighed and transferred to a 10 L Scott bottle. Demineralized water (5 L) was added to this dry mixture to obtain a slurry, which was intensively mixed with a top-mounted propeller mixer (1 h). This slurry was then similarly filtered using a Buchner filter with vacuum, dried and crushed as pure organosolv lignin. To verify the actual composition of the lignin/clay mixture, 5 g of dried particles were placed (duplicate) overnight inside a muffle furnace (AAF 1100, Carbolite Gero, United Kingdom) at 650 °C. From the mass of residues (Fig. 2 in ESI†) after oxidation, the clay and lignin content of the mixture were obtained.

2.2.2. Addition of calcium hydroxide. Lignin (1 kg) was mixed with calcium hydroxide (≥96 wt%, Carl Roth Belgium) to reach a concentration of 20 wt% calcium hydroxide, instead of the 5 wt% as stated by Zhou *et al.*[52] This was done to amplify the effect of calcium hydroxide. Water (5 L) was added to this mixture and the slurry was filtered after 1 h of mixing. The exact content of calcium hydroxide retained in the filter cake was determined (in duplicate) by putting 5 g of dried particles into a muffle furnace overnight at 650 °C. From the mass of calcium oxide[52,56] after oxidation (Fig. 2 in ESI†), the quantity of calcium hydroxide in the filter cake-derived particles was derived. An extra similar gram-scale preparation for comparative TGA/DSC analysis was performed to obtain 5 wt% calcium hydroxide in the lignin.

2.2.3. Addition of sodium formate. A lignin/sodium formate mixture (1 kg) was prepared for lab-scale pyrolysis by adding 500 g of lignin and 500 g of sodium formate in a 10 L Scott bottle. Water was added (5 L) to obtain a slurry by intensive mixing (1 h). To prevent leaching, this slurry was not filtered. Instead, this slurry was first air-dried (48 h) and subsequently oven-dried at 75 °C until dry. The dried solids were again manually crushed to obtain particles of size 2–4 mm for subsequent pyrolysis. To verify the effective quantity of retained sodium formate in the dried solids, a pre-weighed fraction of these lignin/sodium formate solids were re-dissolved with water and subsequently filtered and washed to collect the leachate containing all sodium formate. Water was allowed to evaporate and the mass of the residues after leaching was recorded.

2.3. Thermogravimetric analysis/differential scanning calorimetry

Thermogravimetric analysis (TGA) and differential scanning calorimetry (DSC) were performed on pulverized samples, using a thermal analyzer from Setaram (Sensys Evo TG-DSC S60/58129, France) for characterization. The untreated organosolv lignin as well as the lignins with additives and the additives themselves were subjected to TGA/DSC under a nitrogen atmosphere. The TGA/DSC of lignin/sodium formate was difficult (though successful) due to frothing, but the TGA/DSC of pure sodium formate was repeatedly unsuccessful due to extensive foaming and material overflow. Therefore, data from previous work by Meisel *et al.*[57] was considered for sodium formate.

For TGA/DSC analysis, a sample mass of 2–4 mg was put into a quartz crucible, depending on the lignin content of the sample and its frothing tendency. Each TGA/DSC experiment started with a heating phase (10 °C min^{-1}) from ambient temperature to 30 °C (kept for 3 min to stabilize). The sample was then heated from 30 °C to 105 °C (10 °C min^{-1}) and kept for 10 min. Heating was then initiated at 10 °C min^{-1} from 105 °C to 800 °C, after which it was cooled to ambient temperature.

2.4. Analytical pyrolysis (py-GC/MS)

Analytical pyrolysis was performed on the pulverized lignin samples with and without the additives. For the py-GC/MS analysis, a Tandem Pyrolyser RX-3050-TR unit with an HP 3050 Flow Controller (Frontier Laboratories Ltd) was coupled to a gas chromatograph and mass spectrometer (Thermo Fisher Scientific Trace GC Ultra and Thermo ISQ MS). Between 300 and 600 μg of a sample (depending on the lignin content) was loaded in a deactivated stainless steel sample cup. The sample cup was dropped into a pre-heated pyrolysis tube. The sample was consequently heated rapidly to the set pyrolysis temperature of 500 °C at a rate of *ca.* 2000 °C s^{-1} (this heating rate is claimed by the manufacturer). The evolved (pyrolysis) vapors were directly swept into the GC *via* a restrictor capillary tube in combination with an open split interface (split ratio 1 : 50) at 250 °C and using helium as the carrier gas (≥99.99 mol%). The GC column was an RTX-1701: Restek, L = 60 m; d_i = 0.25 mm; d_f = 0.25 μm, and the temperature program of the GC oven was as follows: (i) three minutes at a constant temperature of 40 °C, (ii) heating to 280 °C at 5 °C min^{-1}, and (iii) one minute at a constant temperature of 280 °C. The GC-separated compounds were led to a single quadrupole MS for electron ionization. The MS transfer line temperature was 280 °C and the ion source temperature was kept at 230 °C. The MS operating conditions were electron impact ionization at 70 eV and a scan mode with mass-to-charge ratio (m/z) values between 29 and 300 with an acquisition rate of 5 spectra per second.

A peak list with area integration was obtained using the Xcalibur 2.1 software with a baseline factor of 200, an area noise factor of 100, and a peak noise factor of 10. The identified compounds were manually annotated, based on their retention times and fragmentation patterns (compared with the National Institute of Standards and Technology (NIST) database, version 2.3). Data were expressed on relative peak area (area%) and peak area per mass lignin (area per μg of lignin). The relative peak area highlights the differences in the volatile fraction's composition, whereas the peak area per mass lignin takes the extent of volatilization into account.

2.5. Melting, softening, and carbonization

To evaluate the effect of the lignin additives on the thermal behavior of lignin (melting, softening, and carbonization) at pre-pyrolysis temperatures, samples were placed on a Kofler bench (Wagner and Munz, Germany), which is in essence a metallic plate with a temperature gradient ranging from room temperature to 265 °C. This allowed the visual observation of changes in structure, color, and consistency over the temperature range. The Kofler bench was calibrated with adipic acid (melting temperature of 150.6 °C) and dicyandiamide (melting temperature of 209.4 °C) as standards (Chempur, Germany).

2.6. Lab-scale pyrolysis

Lab-scale pyrolysis of lignin with and without the different additives was performed in duplicate, using a mechanically agitated fluidized bed reactor (Fig. 1). The ribbon-type mixer allowed a lower nitrogen sweep gas rate to achieve fluidization of the sand bed. Hence, the pyrolysis vapors were less diluted with nitrogen gas for easier condensation. Moreover, the mechanical agitator offers the additional advantage that potential sand/char agglomerates are crushed.

During the operation for biomass pyrolysis, the feedstock in the hopper (1) is usually introduced into the reactor through conveyors (2) and (3), shown in Fig. 1. For lignin pyrolysis, this however proved unsuccessful due to the brittleness of the organosolv particles from the filter cake, resulting in sticky dust-like particles. For lignin with *e.g.*, clay, screw-feeding during preliminary tests was only partly successful, due to the occasional blockages at the reactor entrance after passing the last part of the water-cooled reactor screw (4). Therefore, a lock-hopper system, used to introduce sand to the reactor (9), was used to introduce *ca.* 5 g of lignin (with additives) every 5 minutes into the reactor.

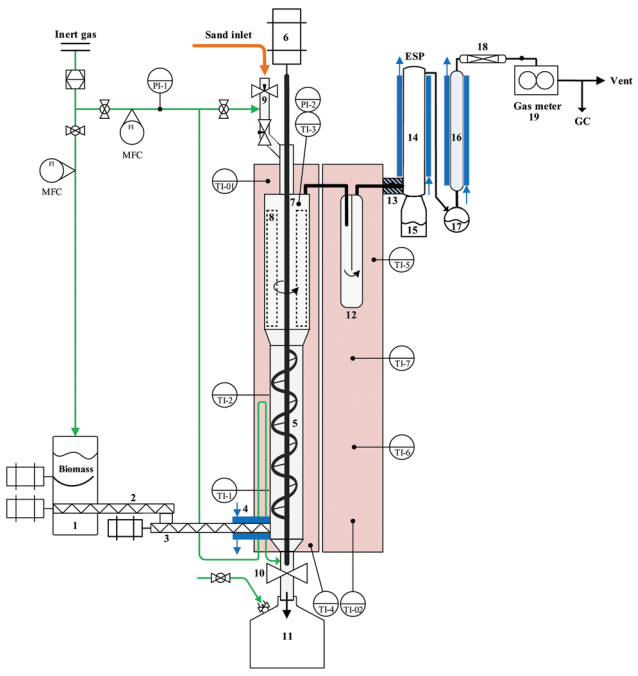

Fig. 1 Mechanically agitated bubbling bed reactor for semi-continuous fast pyrolysis.

The pyrolysis temperature was set to 500 °C for all experiments. A mass of 1.5 kg of sand was loaded into the reactor before the experiment. The average nitrogen sweep gas rate was 283 ± 32L_N per hour. The ribbon mixer (5) was operated during an experiment. Fine entrained char and sand particles were largely removed from the pyrolysis vapor stream by the knock-out vessel (12). After leaving the hot reactor compartments, pyrolysis vapors were led over an insulated tube to an electrostatic cooler (4 °C) and the majority of pyrolysis liquids were recovered in the collection vessel (15). Residual uncondensed vapors were led to a second glass condenser (16) at 4 °C. The uncondensable gases were passed through a cotton wool filter (18), their volumetric flow rates were measured with a wet gas meter (19) (Ritter, Germany), and their compositions were sampled with a micro GC.

2.7. Lignin and products analyses

2.7.1. Elemental analysis. Elemental analysis was performed in triplicate using a Flash 2000 Elemental Analyzer (Thermo Fisher Scientific, Waltham, MA, USA) and 2 mg of each sample. For all samples, the organosolv lignin and liquid pyrolysis products, elements C, H, N, and S were measured, while the oxygen content was obtained by difference. 5-Bis(5-*tert*-butyl-benzoxazol-2-yl)thiophene (BBOT) was used as the standard reference.

2.7.2. GCxGC-FID and GCxGC-HR-ToF-MS analysis. The GC-detectable fractions of the aqueous and heavy phase pyrolysis liquids were analysed using both GCxGC-FID and GCxGC-ToFMS analyses. GCxGC-ToFMS was used for compound identification, whereas GCxGC-FID was used for compound quantification. The GCxGC-FID was calibrated for a number of compounds typically present in pyrolysis liquids. For compounds that were not directly calibrated, response factors from calibrated compounds that share a structural similarity were used.

GCxGC-FID analyses were performed using a Thermo Finnigan Trace GC Ultra equipped with two capillary columns, *i.e.* an RTX-1701 capillary column (L = 30 m; d_i = 0.25 mm; d_f = 0.25 μm) connected by a pressfit to an Rxi-5Sil MS column (L = 120 cm; d_i = 0.15 mm; d_f = 0.15 μm) and a flame ionization detector (FID), set at 280 °C. The injector temperature was 280 °C (1 : 50 split ratio). A liquid CO_2 modulator was applied to trap the samples after passing through the first column. Helium (Linde Gas Benelux 99.995%) was used as the carrier gas (flow rate of 0.8 mL min^{-1}). The temperature program of the GC oven was as follows: first, the temperature was kept at 40 °C for 5 minutes, after which it was increased (3 °C min^{-1}) to 250 °C. The modulation time was 6 seconds. A volume of 1 μL of sample was injected, this being pyrolysis liquid dissolved in tetrahydrofuran (THF) (dilution factor *ca.* 30 for heavy phase, 10 for aqueous phase). di-Butylether was added to THF at a concentration of 500 mg kg^{-1}. The samples were diluted with the DBE spiked THF.

GCxGC-HR-ToF-MS analyses were performed using an Agilent Technologies 7890B GC instrument with a JEOL AccuTOF GCv 4G as the detector. Helium (99.999%) was used. Both the MS interface temperature and the ion chamber temperature were 280 °C. Electron ionisation was performed at 70 eV and the NIST database (version 2.3) was used for compound identification. The second column passes through a modulator with a trap, starting at −50 °C (45 minutes) followed by an increase to 9 °C at a rate of 20 °C min^{-1}.

2.7.3. Gel permeation chromatography. Gel permeation chromatography (GPC) was performed to evaluate the changes in the molecular weights between the as-received organosolv lignin and the heavy pyrolysis liquids which are not GC-detectable. GPC was performed to assess the non-GC-detectable fraction of the heavy pyrolysis liquids, using a Hewlett Packard 1100 Series system equipped with a GBC 1240 RID refractive index detector. Three Agilent Technologies PLgel mixed E columns (L = 300 cm; d_i = 7.5 mm; and d_f = 3 μm) at 40 °C were configured in series. Polystyrene was used as the standard for calibration. The samples were prepared by dissolving 0.05 g of lignin or heavy liquids in 4 mL of tetrahydrofuran (THF). A trace amount of toluene was added as the retention marker. Prior to the injection of 20 μL, the whole sample was filtered (pore size of 0.2 μm). For quantification of the molecular weight distribution, the PSS WinGPC UniChrom software was used.

2.7.4. Heteronuclear single quantum coherence (HSQC) NMR. Heteronuclear single quantum coherence (HSQC) NMR spectroscopy was performed using a Bruker Avance NEO 600, with a 600 MHz (14.1 T) UltraShield Magnet. ^{1}H NMR spectra were acquired using a sweep width of δ 11 ppm. ^{13}C spectra were acquired using a sweep width of δ 220 ppm. Approximately 0.3 g of the heavy liquids was dissolved in *ca.* 1.4% deuterated dimethyl sulfoxide (DMSO-d_6). For comparative semi-quantitative data analysis, the spectra were loaded into Matlab 2019b. The peak for DMSO was removed and the spectra were normalized to have a total signal intensity of unity. Two normalized NMR spectra i and j from two different heavy phases were then mutually subtracted: $I^{i}_{\delta_H,\delta_C} - I^{j}_{\delta_H,\delta_C}$, where $I^{i}_{\delta_H,\delta_C}$ denote the normalized intensity I of spectrum i at a certain position (δ_H, δ_C).

2.7.5. Non-condensable gas analysis. The gases were analyzed with a micro GC Varian 4900 instrument equipped with two analytical columns. The first column was a 10 m Molesieve 5 Å with backflush, which is connected to a heated injector and to a TCD detector using high-purity He as the carrier gas (≥99.999 purity, Air Products, Belgium). The second column was a 10 m PPQ column, also connected to a heated injector and to a TCD detector using high-purity Ar and He as carrier gases. The first column separated and quantified (vol%) H_2, O_2, N_2, CH_4, and CO (in order of occurrence), while CO_2, C_2H_4, C_2H_2, C_3H_6, and C_3H_8 were separated and quantified (vol%) in the second column.

2.8. Calculations and data analysis

2.8.1. Product yields and mass balance. The yield of pyrolysis liquids (both aqueous and heavy) was determined from (i) the mass of the electrostatic precipitator (14) and two collection vessels (15 and 17) in Fig. 1 before and after the experiments and (ii) the quantity of fed lignin. The quantity of the additives and lignin in the prepared samples was calculated from the residues upon oxidation at 650 °C (for lignin/attapulgite and lignin–calcium hydroxide) or the mass of sodium formate recovered from the leachate (section 2.2).

The aqueous phase pyrolysis liquid was decanted from the heavy phase. The mass of the aqueous phase was directly measured from which its yield was calculated. The mass of the heavy phase was obtained by difference to take into account the hard-to-recover heavy phase at the walls of the electrostatic precipitator.

The yield of non-condensable gases was obtained from the difference between (i) the total volume of gas at the outlet of the reactor and (ii) the supplied volume of the nitrogen sweep gas. From the volumetric gas compositions (by micro GC), the ideal gas law, and the specific molecular weight of measured compounds, the yield of non-condensable gases was calculated.

The mass of biochar was obtained by difference, due to the difficulty in recovering char from the set-up (especially for char-like chunks due to frothing), and the discrimination of biochar from the additives in the char particles.

2.8.2. Principal component analysis. To identify the compounds that can discriminate lignin from the prepared lignins with additives, principal component analysis (PCA) was performed.[58] PCA is a multivariate statistical technique that reduces the number of dimensions from *e.g.*, 100 compounds to two dimensions (principal compounds) which are a linear combination of the original dimensions.

Since PCA with the compounds' relative peak areas as independent variables mostly led to the same clustering as PCA with the peak area per mass lignin as independent variables, only the former is herein reported.

PCA was performed with the compounds' scaled relative peak area and with unscaled relative peak area as independent variables. If unscaled, the magnitude of the relative peak area dominates in the PCA analysis. As a consequence, changes in the relative peak area of major compounds are emphasized. To pronounce the changes of minor compounds, the relative peak area of each compound over all lignins were scaled to have an average of zero and standard deviation being unity.

3. Results and discussion

3.1. Lignin with additives

The used organosolv lignin was derived from debarked beech wood (*Fagus sylvatica*); it had an ash content below 1%, and an empirical elemental composition of $C_9H_{9.56}N_{0.023}O_{3.06}$, which is typical of lignin. Clay, calcium hydroxide, and sodium formate were added to lignin to improve the pyrolysis of lignin. Table 1 shows the measured (actual) concentration of each additive in the lignins used for lab-scale fast pyrolysis. The measured sodium formate content was slightly higher

Table 1 Anticipated concentrations of additives within the three lignins compared to the measured (actual) concentrations

Additives	Anticipated	Measured
Attapulgite	50 wt%	50 ± 3 wt%
Calcium hydroxide	20 wt%	17 ± 1 wt%
Sodium formate	50 wt%	53 ± 2 wt%

than intended, likely due to the soluble compounds and impurities in lignin (*e.g.*, ethyl β-D-riboside and furfural, Fig. 3 in ESI†) that resulted in an overestimation of the sodium formate content by means of leaching. After the addition of calcium hydroxide, 17 wt% calcium hydroxide was retained, which is close to the 20 wt% prior to water addition and filtration. Thus, only a limited quantity of calcium hydroxide leached out.

3.2. TGA/DSC analysis

Fig. 2 presents a selection of the results from TGA/DSC analysis of lignin with and without additives. TGA/DSC was performed to infer the composition of the lignins with additives.

Among the additives, the clays appeared inert, with virtually no mass loss (TGA in Fig. 4c in ESI†). In contrast, pure calcium hydroxide and sodium formate did show a certain mass loss. For sodium formate, mass loss was the fastest at *ca.* 400 °C and 500 °C and both reactions were exothermic (Fig. 2a and c). However, a very endothermic peak was apparent for sodium formate at *ca.* 250 °C (Fig. 2b and c). Based on Meisel *et al.*[57] our results, sodium formate underwent the following subsequent reactions:

$$2\mathrm{HCOONa} \xrightarrow{250\,^{\circ}\mathrm{C}} \mathrm{Na_2CO_3} + \mathrm{CO} + \mathrm{H_2},$$

$$2\mathrm{HCOONa} \xrightarrow{250\,^{\circ}\mathrm{C}} \mathrm{Na_2C_2O_4} + \mathrm{H_2},$$

$$\mathrm{Na_2C_2O_4} \xrightarrow{400\,^{\circ}\mathrm{C}} \mathrm{Na_2CO_3} + \mathrm{CO},$$

$$\mathrm{Na_2CO_3} \xrightarrow{500\,^{\circ}\mathrm{C}} \mathrm{Na_2O} + \mathrm{CO_2}.$$

The produced hydrogen thus is released from the formate salt at a temperature well below the applied pyrolysis temperature in this study, which is 500 °C.

However, calcium hydroxide had a distinct endothermic mass loss peak at *ca.* 450 °C (Fig. 2a and c), which is associated with the endothermic formation of calcium oxide.[59] The heat flows during the TGA/DSC analysis of all lignins with additives, except sodium formate, were rather similar (Fig. 2b). For lignin with calcium hydroxide, this similarity has important implications. For lignin with calcium hydroxide at application rates (5 wt% and 20 wt%) shown in Fig. 2b, the endothermic formation of calcium oxide from free calcium hydroxide was not observed. This indicates that virtually no free calcium hydroxide remained in the lignin–calcium hydroxide mixture. Hence, all calcium hydroxide did seem to have bound to lignin. For lignin with sodium formate, endothermic and exothermic peaks associated with the dissociation of pure sodium formate were still apparent (Fig. 2b), indicating a solely physical mixture of lignin and sodium formate.

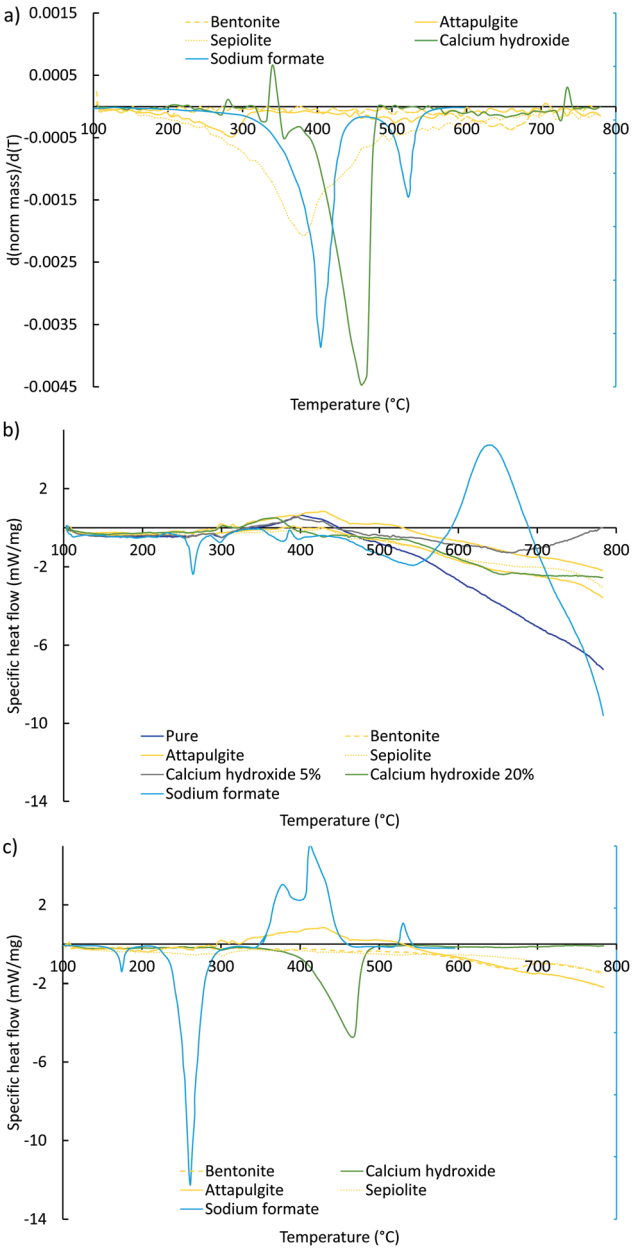

Fig. 2 Results from the heating phase of TGA/DSC analysis. (a) Mass-loss rate of the additives; (b) heat flow (negative: endothermic; positive: exothermic) for lignin with and without additives; and (c) heat flow for additives. Data for mass-loss rate and heat flow from sodium formate are from Meisel *et al.*[57] and presented in arbitrary units. Other TGA/DSC plots are shown in Fig. 4a in ESI.†

Therefore, the following nomenclature was applied throughout the entire manuscript. Lignin/clay and lignin/sodium formate denote a physical mixture, while lignin–calcium hydroxide denotes chemically bound calcium hydroxide to lignin.

3.3. Analytical pyrolysis of lignin with and without additives

Results from analytical pyrolysis provide insights into the primary lignin depolymerization reactions, *i.e.*, without long

hot-vapor residence times and vapor condensation. Thorough data analysis from analytical pyrolysis was performed to identify the (subtle) differences among the lignins which, along with the analysis of the pyrolysis liquids from lab-scale pyrolysis, allowed to design experiment-based putative pyrolysis mechanisms with a distinction between primary and secondary reactions. Fig. 5 in ESI† shows the representative pyrograms. The complete list of compounds, along with the average values and standard deviations for the relative peak areas (area%) and peak area per mass lignin (area per μg), are provided in Tables 1 and 2 in ESI.†

Fig. 3a shows the lignin samples (*i.e.*, individuals) on a two-dimensional plane with the principal components (PC) as axes and the evolved compounds' unscaled relative peak area as independent variables. The individual plots with the peak area per mass of lignin as independent variables were similar and are shown in Fig. 6c in ESI.† Fig. 3b represents the individuals in PCA analysis with the relative peak area for scaled data, *viz.*, without taking the order of magnitude in relative peak areas into account. Data points in close proximity in Fig. 3a indicate the similarities between the evolved major compounds from the lignin samples. Data points in close proximity in Fig. 3b indicate the similarities among all compounds (minor and major) from the lignin samples. Three groups were discriminated in Fig. 3a, which are (i) pure lignin + lignin/clays, (ii) lignin–calcium hydroxide, and (iii) lignin/sodium formate. The inclusion of minor compounds in PCA analysis resulted in the separation of pure lignin and lignin/clays along PC2 (Fig. 3b).

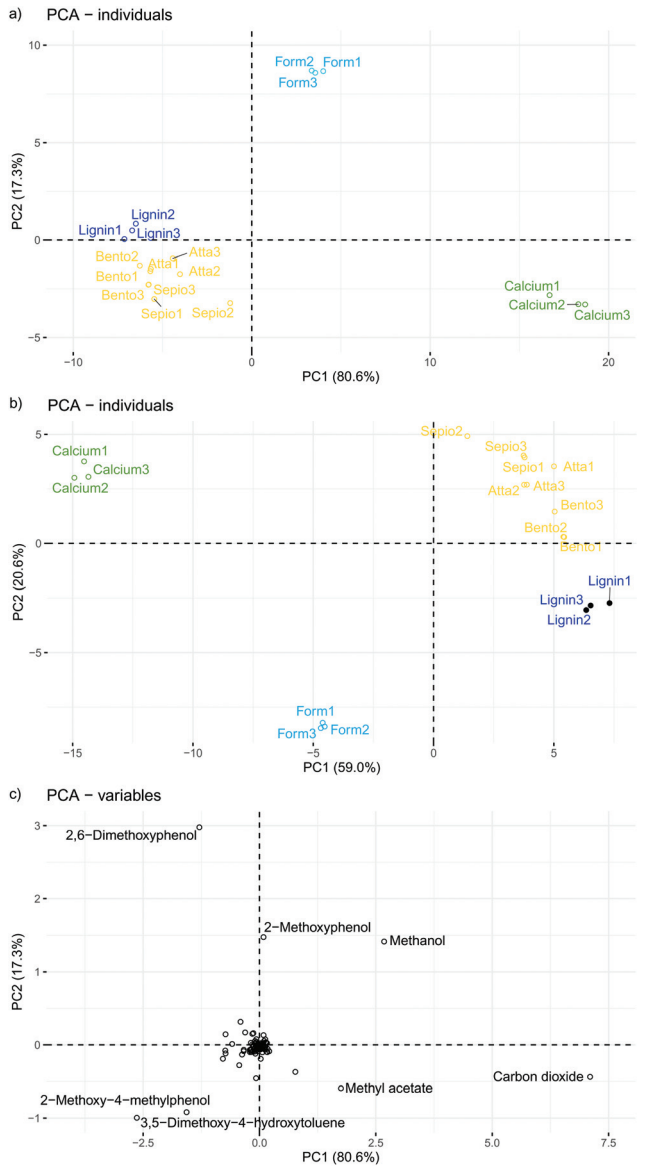

Fig. 3 Individual (a and b) and variable (c) plots from principal component analysis, using pure lignin and lignins with additives as dependent variables and unscaled relative peak area (a and c) and scaled relative peak area (b) as independent variables. All three replicates from analytical pyrolysis are separately plotted.

The compounds responsible for the clustering in Fig. 3a are represented in a variable plot in Fig. 3c. The first principal component in Fig. 3c was mainly directed by the changes in *e.g.*, carbon dioxide and methanol (positive end) and 5-dimethoxy-4-hydroxytoluene (negative end) as major compounds and mainly discriminated lignin–calcium hydroxide from the lignins with additives. Lignin/sodium formate (Fig. 3c) was mostly characterized by the presence of *e.g.*, 2,6-dimethoxyphenol and 2-methoxyphenol (high value for PC2). Per mass of lignin, approximately twice as much more 2-methoxyphenol and 2,6-dimethoxyphenol was detected upon the addition of sodium formate, compared the addition of clay (Table 2 in ESI†). However, lignin–calcium hydroxide showed the lowest area per mass of lignin in those compounds. For the cluster with pure lignin and lignin/clay (Fig. 3a), 3,5-dimethoxy-4-hydroxytoluene and 2-methoxy-4-methylphenol were most notable characteristic compounds.

Upon PCA analysis with scaled relative peak areas, much more (minor) compounds were found to direct the two principal components (variable plot in Fig. 6f in ESI†). The plots in Fig. 4 show the contribution (importance) of the different compounds to the two principal components.

Fig. 4a shows many compounds with almost similar contributions to the first dimension, through which lignin–calcium hydroxide, lignin/sodium formate, and pure lignin + lignin/clays were differentiated. These were mainly highly substituted methoxyphenols and the relative peak area of a selection of those is shown in Fig. 5a. The second dimension shown in Fig. 3c is important; through this dimension, lignin was differentiated from lignin/clay. The responsible components were *e.g.*, 3-methylphenol (Fig. 4b) and methyl- and dimethylphenols, in general (Fig. 4). Fig. 5b and c show these differences in the methyl- and dimethylphenols of pure lignin and lignin/clay (especially attapulgite) by their relative peak area. So, although pure lignin and lignin/clay in a major way share the same pyrogram, subtle differences are present, especially in the methylphenols. Lignin–calcium hydroxide also showed high specificity towards alkylphenols, as they had the highest relative peak area for all methyl- and dimethylphenols.

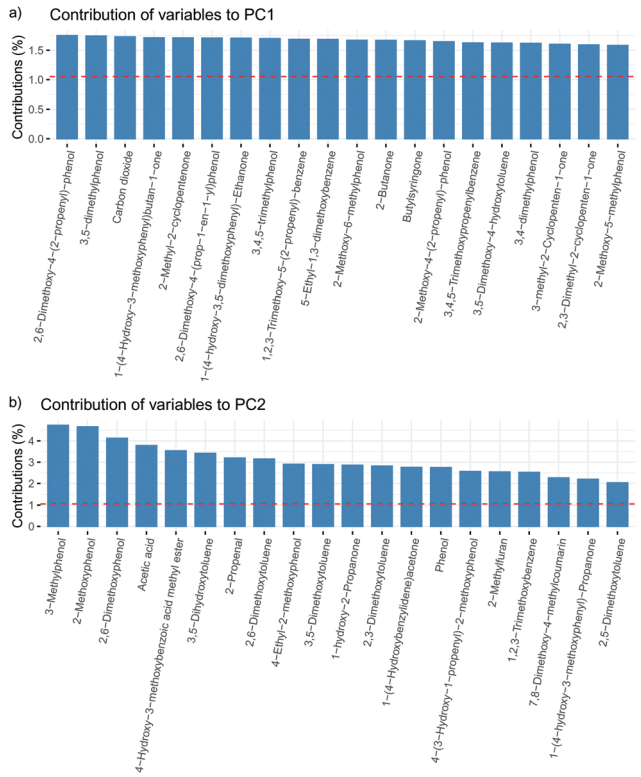

Fig. 4 Contribution of minor and major compounds to principal component 1 (a) and principal component 2 (b) in principal component analysis using the scaled relative peak areas (%) as independent variables and lignin with and without additives as dependent variables.

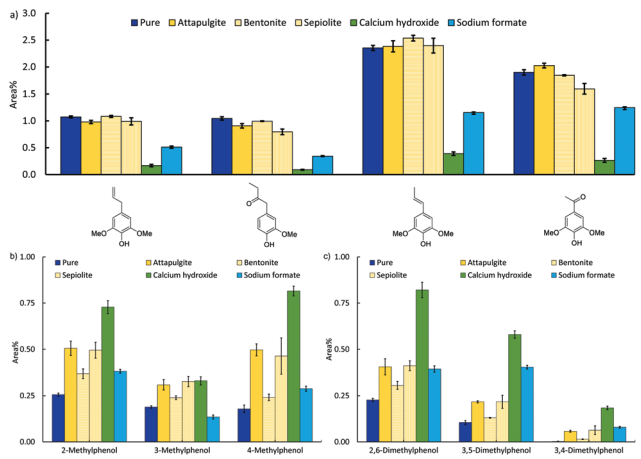

Fig. 5 Relative peak area (%) of minor compounds evolved upon the analytical pyrolysis of lignin with and without additives. (a) Highly-substituted methoxyphenols; (b) methylphenols; and (c) dimethylphenols.

3.4. Pre-pyrolysis softening and melting

Results from the Kofler bench are visualized in Fig. 7 in ESI.† Pure lignin started to discolor at *ca.* 160 °C (accompanied by softening), partially melted at *ca.* 180 °C, and completely melted and carbonized from *ca.* 210 °C in a similar way as reported by Shrestha *et al.*[31] and Montoya *et al.*[60] This melting of pure lignin persisted in lab-scale pyrolysis, causing blockages and so hampering long-term operations (*vide infra*). Every lignin with additive also underwent discoloration, directly followed by carbonization without apparent melting or forming a viscous substance (Fig. 7 in ESI†). Hence, all additives effectively avoided lignin melting.

To enter the liquid phase during melting, mobility of the lignin polymer is required. As the molecular weight of organosolv lignin is among the lowest ones of technical lignins,[61] organosolv lignin polymers can move rather easily upon melting.[60] It was, therefore, assumed that lignin/clay and lignin/sodium formate (each at 50 wt%) hindered the mobility of the lignin polymer. For lignin–calcium hydroxide (20 wt%), this can also hold true. However, the possibility that calcium hydroxide induced cross-linking of different lignin polymers cannot be excluded (see section 3.8.2). Indeed, lignin–calcium hydroxide was the only one that lacked a discoloration phase (accompanied by softening), while[32] showing that increased cross-linking (*i.e.*, decreased mobility) avoids lignin's rubbery flow associated with softening.

3.5. Practical observations during fast pyrolysis

Pure organosolv lignin and lignin with additives were subjected to lab-scale fast pyrolysis in the set-up described in Fig. 1. All liquids were spontaneously phase-separated (Fig. 8 in ESI†).

Fast pyrolysis of pure lignin ceased prematurely due to blockages resulting in a decrease in the condensation of pyrolysis vapors. Only an estimated 95 g of lignin was fed, instead of the envisaged 350 g. Upon disassembling the reactor, it was clear that the blockage was—as expected—caused by lignin's melting tendency and subsequent carbonization of the frothed lignin. Fig. 6 (left) shows a carbonized lignin melt on the axle of the ribbon mixer just at the entrance of the hot reactor zone. Lab-scale pyrolysis with pure lignin was therefore not replicated.

After fast pyrolysis of lignin–calcium hydroxide, small coke-like particles were apparent at the nexus between the bottom of the electrostatic precipitator and the entrance of the liquid collection vessel (Fig. 6, middle). These entrained coke-like particles were likely formed by a more extensive repolymerization of phenolics catalysed by calcium oxide originating from lignin–calcium hydroxide pyrolysis. The sand was retained in the reactor over the course of the experiment. This caused the formed calcium oxide from lignin–calcium hydroxide to also be retained in the reactor and allowed it to engage in catalytic reactions. This is elaborated in section 3.8.2. Pyrolysis of lignin/sodium formate led to the formation of expanded char particles on top of the spacer (no. 8 in Fig. 1 of the set-up) as visualized in Fig. 6. This expanded nature was due to the formation of H_2 and CO as indicated by TGA/DSC analysis.

3.6. Pyrolysis product yields

The yields of pyrolysis liquids, char, and non-condensable gases are shown in Fig. 7. The yield from the pyrolysis of pure lignin is only indicative, as the blockages (Fig. 6) hampered the replication and adequate recording of effectively fed lignin.

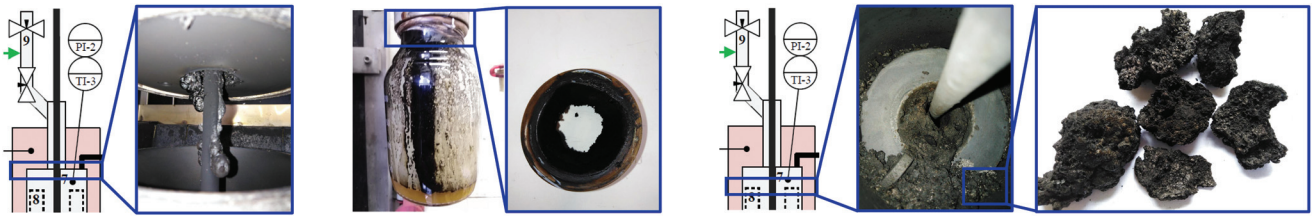

Fig. 6 Important practical observations during the fast pyrolysis of lignin with and without additives. Left: Blockages induced by melting of pure lignin. Middle: Fine entrained char from lignin–calcium hydroxide pyrolysis. Right: Expanded char from pyrolysis of lignin/sodium formate.

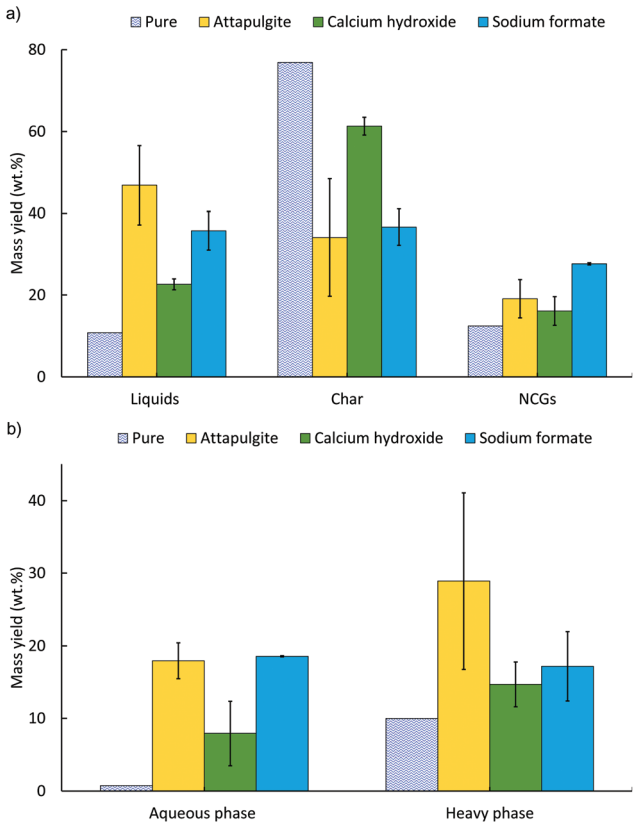

Fig. 7 Product yields (liquids, char, and non-condensable gases) of fast pyrolysis of lignin with and without additives (a) with a distinction between aqueous liquids and heavy liquids (b).

So, the yield of char (obtained by difference) for pure lignin can be slightly lower. However, the clear general tendency towards char formation and modest liquid formation from pure lignin is apparent.

For lignin/attapulgite and lignin/sodium formate, the yield of liquids increased, compared to pure lignin, to *ca.* 35–45%. These liquid yields were similar, yet slightly higher than those reported in the literature (33–37 wt% for lignin/clay[46] and 28.5–32.5 wt% for lignin/sodium formate[49]). The yield of liquids from lignin–calcium hydroxide was the lowest and also modestly overestimated, as the fine entrained solids in the electrostatic cooler in Fig. 6 were also considered heavy liquids. In any case, the addition of calcium hydroxide (20 wt%) did result in less liquids (22.6 wt%) than from the pyrolysis of lignin–calcium hydroxide (5 wt% $Ca(OH)_2$), being *ca.* 38 wt%.[52] According to the current working mechanism,[52] any additional presence of calcium hydroxide would go in tandem with an increase of lignin–ϕ–O–CaOH bonds, that should facilitate pyrolysis. Not observing any benefit from the higher dose of calcium hydroxide is undoubtedly due to the different dose of calcium hydroxide and its associated structural changes (section 3.8.2).

Regarding the distribution of the pyrolysis liquids, it was observed that in all cases, except for lignin/sodium formate, the yield of the heavy phase was higher than that of the aqueous phase (Fig. 7b). For pure lignin, there was virtually no aqueous phase recovered.

The volumetric composition of the non-condensable gases (on a nitrogen-free basis) is presented in Fig. 8. While pure lignin resulted mostly in carbon dioxide and methane, the profiles of non-condensable gases from pyrolysis of lignin with additives were more diversified. Both H_2 and CO were characteristic for lignin/sodium formate, due to the thermal decomposition of the formate salt. Furthermore, lignin–calcium hydroxide also shows a rather hydrogen-rich off-gas, which was absent for lignin/attapulgite. Hence, a clear difference in the mechanisms should be expected (*vide infra*).

All of the gases in Fig. 8 also bear significant energy. These off-gases can be combusted to deliver the required heat for

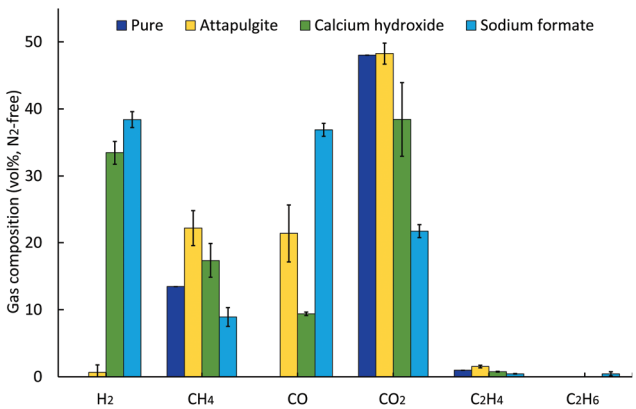

Fig. 8 Composition of the non-condensable gases (on nitrogen-free basis) on volume basis for lignin with and without additives during fast pyrolysis.

pyrolysis and so lowering the energy demand of the whole process.

3.7. Pyrolysis liquid composition

The heavy pyrolysis liquids were of main interest, as these contain the monoaromatic compounds relevant to the chemical industry. Typically, a non-monomeric energy-dense fraction is also present, which also holds the potential for further upgrading. The aqueous and heavy liquids were analysed through elemental analysis, while the heavy phase was analysed with GPC to assess the contribution of dimeric and oligomeric compounds. The monomeric compounds themselves were analysed in detail *via* GCxGC-FID and GCxGC-ToFMS analysis. The functionalities of the whole heavy liquids were analysed through HSQC analysis.

3.7.1. Elemental composition. The elemental compositions of the heavy phase of the pyrolysis liquids are presented in Table 2, along with their atomic H/C and O/C ratios. It is clear that the heavy phase of pure lignin was most carbon dense, having *ca.* 70 wt% of carbon. Moreover, the heavy phase from lignin–calcium hydroxide was also the most deficient in hydrogen, leading to the lowest hydrogen/carbon ratio of 1.08. This points to a high fraction of condensed aromatic structures with a low H/C ratio in the heavy pyrolysis liquids. Further aromatization and condensation during pyrolysis, with calcium oxide as the catalyst, could have led to the formation of the observed fine char particles and can explain the relatively high evolution of hydrogen gas associated with the aromatic ring condensation and the observed fine particles after the experiment.

In contrast, the heavy phase from lignin/attapulgite and lignin/sodium formate showed a decreased carbon content (*ca.* 57–58 wt%) and increased oxygen content (*ca.* 33–35 wt%), compared to that of pure lignin. This points to the direction of more oxygenated compounds in the heavy phase. For the heavy phase from lignin/sodium formate pyrolysis, the highest hydrogen content was observed. This already illustrates that hydrogen from the sodium formate has been effectively incorporated into the heavy phase compounds, which also was observed by Li *et al.*[48] The aqueous phase of all the analyzed samples were expectedly very carbon-poor (between 2.28 wt% and 4.23 wt%, Table 3 in ESI†), while being oxygen- and hydrogen-rich.

3.7.2. GCxGC-FID and GCxGC-HR-ToF-MS. Table 3 shows that the GC-detectable fraction in the heavy phase was substantial (*ca.* 19–27 wt%), which for the aqueous was rather marginal (between 0.52 and 1.19 wt%, Table 4 in ESI†). Representative raw 2D chromatograms are shown in Fig. 9 in ESI†, and show that the groups of compounds in Table 3, especially alkylphenols, catechols, and guaiacols, comprise ample individual compounds.

Table 3 Concentrations of various groups of GC-detectable compounds (wt%, liquid basis) in the heavy phase after pyrolysis of lignin with and without additives. Hydrocarbons are both branched and linear; PAHCs are polyaromatic hydrocarbons; ket./aldeh. are ketones and aldehydes

	Pure	Attapulgite	$Ca(OH)_2$	HCOONa
Alkylphenols	7.27	9.06	12.91	10.62
Catechols	10.36	5.97	7.14	2.13
Guaiacols	5.13	3.84	3.75	3.93
Acids	0.50	0.46	0.42	0.93
Hydrocarbons	1.50	0.64	0.33	0.02
Cycloalkanes	0.00	0.00	0.00	0.00
Ket./aldeh.	0.70	0.67	1.57	0.87
Aromatics	0.20	0.21	0.15	0.14
PAHCs	0.26	0.40	0.75	0.25
Total	25.91	21.25	27.02	18.89

The fraction of GC-detectable compounds in the heavy phase liquids from lignin–calcium hydroxide was the highest among the lignins (Table 3). So, despite the rather limited yield in heavy liquids (Fig. 7), the liquids themselves are of high interest due to the increased quantity of alkylphenols and catechols. Lignin–calcium hydroxide also showed the highest yield in naphthalenes and polyaromatic hydrocarbons (like fluorene and 2-methyl-9*H*-fluorene) on heavy liquid basis. This also shows an increased selectivity towards polyaromatic ring structures that, if persisting in larger polyaromatic structures, can explain the low H/C ratio from elemental analysis and eventually the formation of the observed small char particles during pyrolysis. Lignin/sodium formate and lignin/attapulgite resulted in a heavy phase with a more modest GC-detectable fraction (*ca.* 19 wt% and 21 wt%, resp.), but which was rich in alkylphenols. The reason for these lower volatile fractions is the slightly higher water content in those phases as also evidenced by the higher O/C and H/C ratios (Table 2).

In Fig. 9, the carbon yield in the heavy phase is plotted against the mass yield in functional monoaromatic compounds such as alkylphenols, catechols, and guaiacols (Table 3). These volatile compound groups can be recovered and upgraded to fuel additives or other chemical intermediates. The best lignin additive would result in a heavy phase that lies at the upper right corner, *viz.* having high carbon and monomer yields. Yet, none of the additives were high for both features. The heavy phase from lignin/attapulgite pyrolysis had the highest carbon yield, yet, a modest monomer yield. For the pyrolysis of lignin–calcium-hydroxide, the opposite was true.

Table 2 Elemental analysis of the heavy phase from pyrolysis of lignin with and without additives

Heavy phase	C (wt%)	H (wt%)	N (wt%)	O (wt%)	H/C	O/C
Pure	69.54 ± 1.37	6.53 ± 0.25	1.49 ± 0.11	22.45 ± 1.50	1.13	0.24
Lignin/attapulgite	57.83 ± 0.50	6.06 ± 0.09	1.04 ± 0.02	35.06 ± 0.39	1.26	0.45
Lignin–calcium hydroxide	66.42 ± 0.01	5.96 ± 0.00	1.63 ± 0.07	25.99 ± 0.07	1.08	0.29
Lignin/sodium formate	57.15 ± 0.20	8.65 ± 0.05	1.42 ± 0.04	32.77 ± 0.22	1.82	0.43

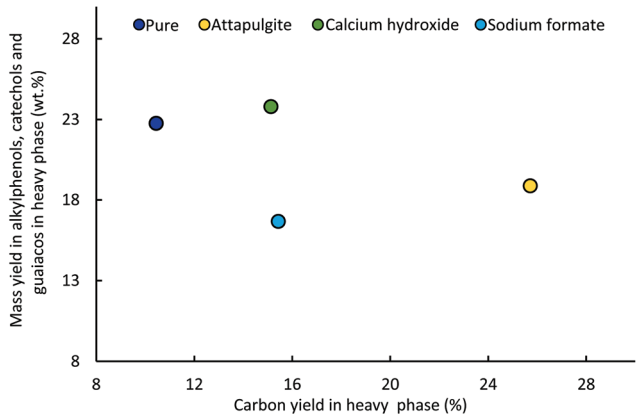

Fig. 9 Carbon yield *versus* the monomer yield of the heavy liquids from lignin with and without additives.

Hence, if the valorization potential of the substantial non-volatile liquid fraction to energy fuel or carbon materials is also considered, the tested lignins can be ordered according to their valorization potential as lignin/attapulgite > lignin–calcium hydroxide > lignin/sodium formate > pure lignin.

Rather than the nine groups of compounds listed in Table 3, Fig. 10 shows a more detailed profile of the heavy phase composition. Consistent with analytical pyrolysis, lignin–calcium hydroxide predominantly resulted in methylphenols, dimethylphenols, and trimethylphenols *i.e.*, alkylphenols (Fig. 10). These alkylphenols constituted the largest distinguishable fraction in the pyrolysis liquids for all lignins. The group of methoxyphenols (alkylated and non-alkylated) in the heavy liquids were not predominantly present, but a selectivity towards these compounds from lignin/sodium formate was apparent (Fig. 10). Ethylmethylphenols were also detected in the heavy liquids at meaningful quantities for all lignins, but were not detected during analytical pyrolysis. This is due to the inherent differences between analytical pyrolysis and reactor-scale pyrolysis with longer hot-vapor residence times, vapor condensation, and possible ageing of the liquids.

As lignin/attapulgite and lignin-calcium hydroxide yielded the most interesting heavy phases in terms of carbon yield and total monomeric aromatics, it is now important to evaluate the absolute yield of very specific and easily recoverable compounds per mass of lignin. Indeed, a number of compounds present in the heavy phase hold value as such. Interesting compounds are cresylic acid (phenol, cresols, and xylenols) and methoxylated benzene/phenol. Cresylic acid finds direct applications as *e.g.*, disinfectants and wood preservatives, while cresols are intermediates for *e.g.*, 2,6-di-*tert*-butyl-*p*-cresol (BHT) and 4-chloro-*o*-cresol (selective plant protecting agents[62]). Several methoxyphenols can be selectively extracted for further utilization[63] or the pooled group can be deployed as a starting material for *e.g.*, polyols and polyurethane foams.[64] Also, these compounds hold value as fuel (additives) if produced at larger quantities.

Table 4 presents the yield on lignin-basis (wt%) of those two industrially relevant products. While the heavy phase from lignin/attapulgite provided the highest carbon yield and a moderate yield of total monoaromatic compounds (Fig. 9), most cresylic acid per mass of lignin was obtained from lignin/attapulgite followed by lignin-calcium hydroxide. However, Table 4 also shows that lignin/attapulgite also results in the second-most, yet modest, quantity of methoxylated benzene/phenol. Hence, lignin/attapulgite as a simple additive appears attractive. The order of lignins thus remained lignin/attapulgite > lignin–calcium hydroxide > lignin/sodium formate > pure lignin when considering more individual compounds.

3.7.3. Molecular weight distribution (GPC). The molecular weight distribution of the compounds in the heavy phase liquids is shown in Fig. 11. After pyrolysis, the molecular weight of organosolv lignin shifted from *ca.* 1500 g mol^{-1} to 150–200 g mol^{-1}. The latter range of molecular weight corresponds to putative dimeric structures, presented in Fig. 11. Only a small shoulder at *ca.* 150 g mol^{-1} was apparent after

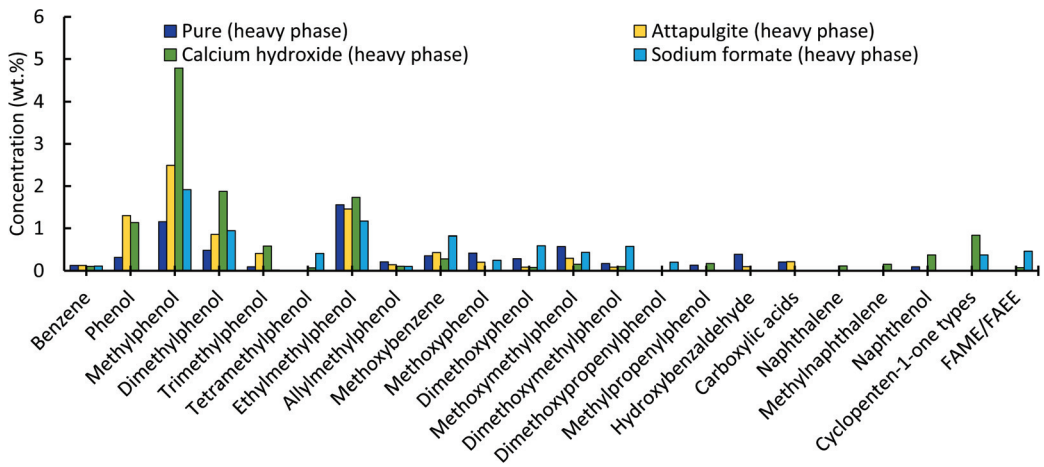

Fig. 10 Concentrations of individual GC-detectable compounds and specific group of compounds (wt%, liquid basis) for the heavy phase after pyrolysis of lignin with and without additives.

Table 4 Yield of cresylic acid (phenol, cresol, xylenol) and methoxylated aromatics (methoxybenzene and methoxy(alkyl)phenols) on lignin basis (wt.%)

	Cresylic acid	Methoxylated aromatics
	wt% (on lignin basis)	
Pure	0.20 ± 0.00	0.18 ± 0.00
Lignin/attapulgite	1.34 ± 0.44	0.32 ± 0.32
Lignin–calcium hydroxide	1.14 ± 0.21	0.09 ± 0.02
Lignin/sodium formate	0.49 ± 0.14	0.46 ± 0.13

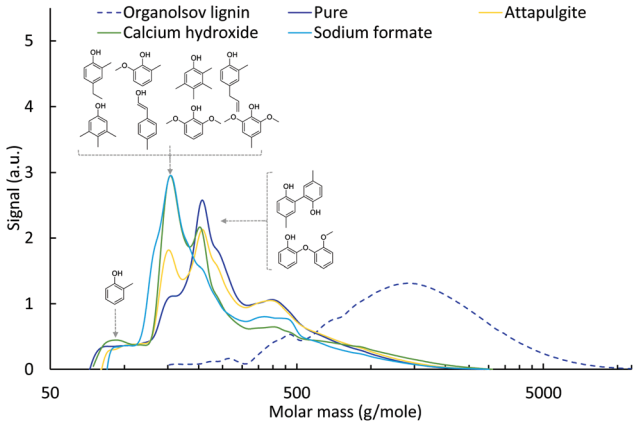

Fig. 11 Distribution of the molecular weight (g mol^{-1}) in the heavy liquids upon pyrolysis of lignin with and without additives.

the pyrolysis of pure lignin. In contrast, the peak at a molecular weight of 150 g mol^{-1} was much more prevalent for all lignins with additives, being the highest for lignin/sodium formate and lignin–calcium hydroxide, followed by lignin/attapulgite. The various compounds detected by GCxGC analysis that fall into the range of that prominent peak (100–200 g mol^{-1}) are annotated in Fig. 11.

Interestingly, the heavy phase from lignin/sodium formate was the only one that lacked a peak associated with the dimeric structures in Fig. 11 at a molecular weight of 200–250 g mol^{-1}. This could be a direct consequence of *in situ* hydrogen that could quench radical intermediates (*e.g.*, quinone methide) from lignin pyrolysis, and so prevent their repolymerization to *e.g.*, 2-(2-methoxyphenoxy)phenol and biphenolic compounds shown in Fig. 11.

While individual compounds are often of interest, the heavy liquids as a whole present value as fuel. Indeed, a carbon-rich (hence energy-rich) liquid is obtained that is logistically more interesting than solid biomass for transportation. Moreover, after the recovery of low-molecular-weight compounds, a significant carbon-rich residue remains that also can be used as an energy carrier and feedstock for carbon materials[65] and can even be upgraded (though hydrotreatment) into additional phenolic compounds.[66]

3.7.4. HSQC 2D NMR. To pronounce the differences and mutually compare the HSQC NMR spectra of the different heavy liquids, all spectra were normalized and mutually subtracted. The raw HSQC NMR spectra are shown in Fig. 10 in ESI.† Fig. 12 shows the results from subtracting the spectra $I^{i}_{\delta_H,\delta_C} - I^{j}_{\delta_H,\delta_C}$, where $I^{i}_{\delta_H,\delta_C}$ denotes the normalized intensity I of the spectrum i at a certain position (δ_H, δ_C). The spectra i and j that were subtracted are indicated by the individual titles in Fig. 12. Plot "Attapulgite-pure", for instance, is the result of lignin/attapulgite's heavy phase spectrum minus the spectrum of pure lignin's heavy phase.

The six plots in Fig. 12 focus on the methoxyl groups: δ_H from 3 to 4.2 ppm and δ_C from 46 to 66 ppm. As anticipated from the studies by Ben and Ragauskas[67] and Hao *et al.*[68], two rather distinct methoxyl moieties (ϕ-OCH_3) were apparent on (substituted) benzene/phenol compounds. They were located at (i) δ_H = 3.74 ppm; δ_C = 56 ppm and (ii) δ_H = 3.84 ppm; δ_C = 56 ppm. Those two methoxyl moieties respectively represent those from (i) methoxybenzene or methoxybenzene with an alkyl moiety in the *para* position, like in 1,2-dimethoxybenzene or (ii) 2-methoxyphenol. The subtraction of the spectrum for the heavy phase from lignin/sodium formate with that of (i) pure lignin, (ii) lignin/attapulgite, or (iii) lignin/calcium hydroxide (bottom row in Fig. 12) indicates the existence of another distinct methoxyl moiety with a slightly lower δ_H = 3.70 ppm. The position is characteristic of the methoxyl group in *e.g.*, 4-methyl-2,6-dimethoxyphenol (δ_H = 3.73 ppm; δ_C = 56.1 ppm), which was also most pronounced for the heavy liquids from lignin/sodium formate pyrolysis in Fig. 10. Plots of "$Ca(OH)_2$-pure" and "$Ca(OH)_2$-attapulgite" shown in Fig. 12 also confirm the relative lack of methoxyl moieties in heavy liquids from lignin–calcium hydroxide pyrolysis, since those plots had very negative intensities associated with the methoxyl regions.

Fig. 13 focuses on the aromatic C–H region. Pyrolysis of lignin–calcium hydroxide resulted in the formation of polyaromatic compounds in the heavy phase liquids. This was apparent from a series of positive peaks in plots "$Ca(OH)_2$-pure" and "$Ca(OH)_2$-attapulgite" and a series of negative peaks in "sodium formate-$Ca(OH)_2$" in the range of δ_H = 7.5–8 ppm and δ_C = 125–130 ppm. This range is typical for C–H in *e.g.*, naphthalene or fluorene. This supports the observations from the GC analysis of the heavy liquids shown in Fig. 10 as well as the relatively high contribution of hydrogen gas in the non-condensable gases as shown in Fig. 8. The pronounced presence of phenol in the heavy phase from lignin–calcium hydroxide and lignin/attapulgite pyrolysis was also apparent. The characteristic peaks for C–H in phenol at the *ortho* position (δ_H = 7.2 ppm; δ_C = 130 ppm) and *meta* position (δ_H = 6.8 ppm; δ_C = 115 ppm) were clearly visible in plots "attapulgite-pure" and "$Ca(OH)_2$-pure" shown in Fig. 13. The high contribution of dimethoxy(methyl)phenols in the heavy liquids from lignin/sodium formate pyrolysis was reflected in pronounced peaks at δ_H = 6.6 ppm and δ_C = 106 ppm, characteristic of C–H at the *meta* position (to ϕ-OH) in dimethoxy(methyl)phenols.[67]

3.8. The pyrolysis mechanism of lignin with and without additives

3.8.1. Lignin/attapulgite. As shown in Fig. 10, the phenol and methylphenol concentrations differed between lignin/

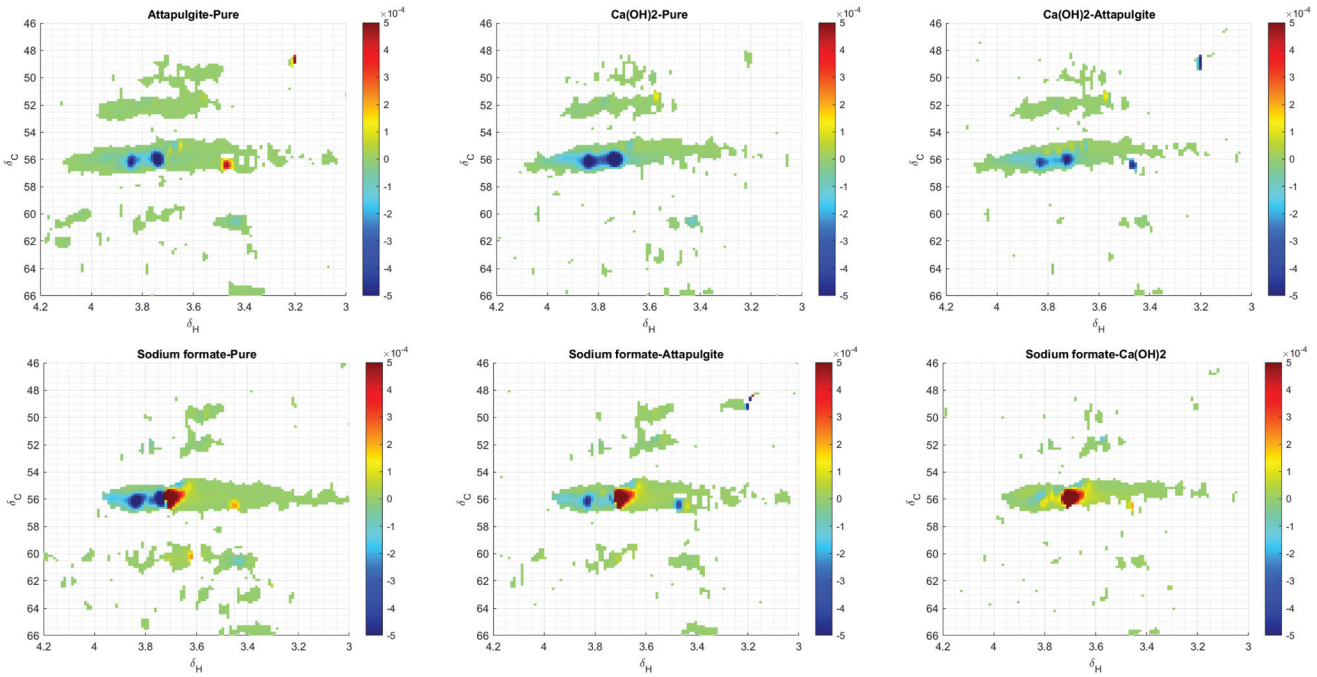

Fig. 12 Results of HSQC NMR analysis, focusing on the methoxyl zone. The plots show the results of subtracting the spectra $I^{i}_{\delta_H,\delta_C} - I^{j}_{\delta_H,\delta_C}$, where $I^{i}_{\delta_H,\delta_C}$ denotes the normalized intensity I of spectrum i at a certain position (δ_H, δ_C). The spectra i and j that were subtracted are indicated by the individual titles.

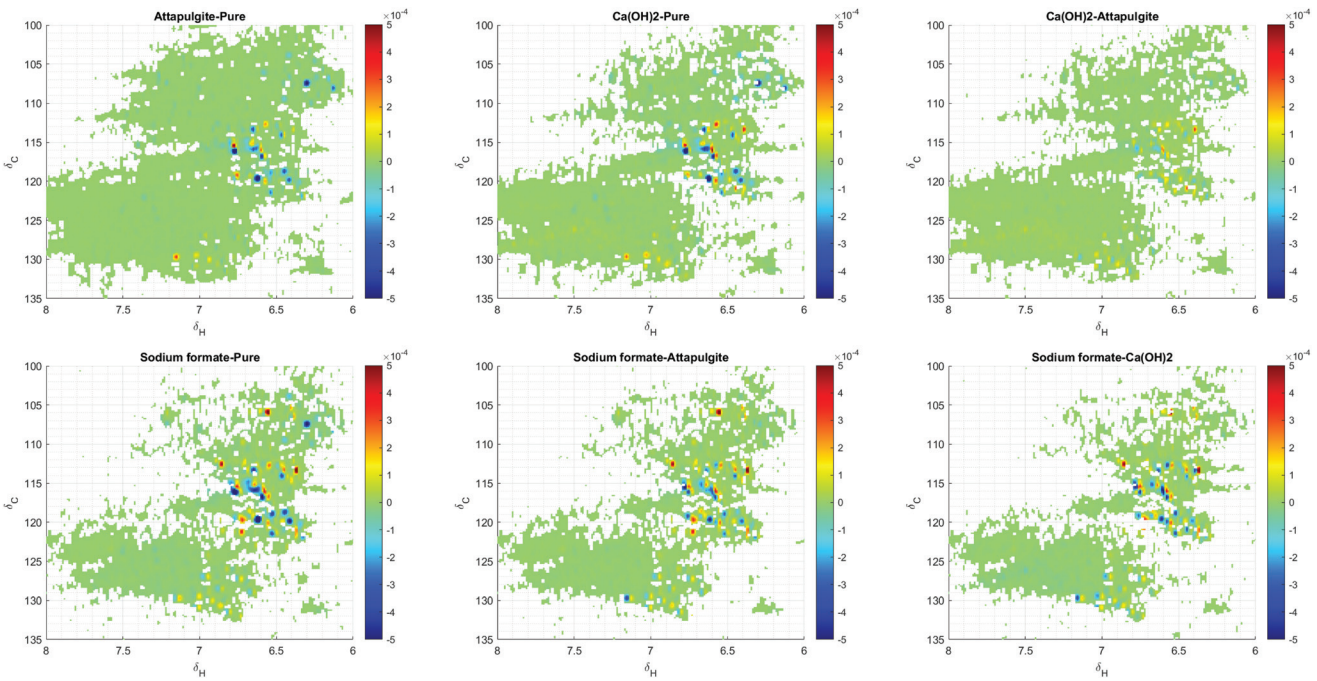

Fig. 13 Results of HSQC NMR analysis, focusing on the aromatic C–H zone. The plots show the results of subtracting the spectra $I^{i}_{\delta_H,\delta_C} - I^{j}_{\delta_H,\delta_C}$, where $I^{i}_{\delta_H,\delta_C}$ denotes the normalized intensity I of spectrum i at a certain position (δ_H, δ_C). The spectra i and j that were subtracted are indicated by the individual titles.

attapulgite-derived heavy liquids and pure lignin-derived heavy liquids. This was also confirmed from the second dimension of PCA analysis (that discriminated pure lignin from lignin/attapulgite) shown in Fig. 4b. The phenol and methylphenol concentrations were also high for the pyrolysis of lignin–calcium hydroxide. Yet, two distinct reaction mechanisms were proposed, motivated by *e.g.*, the co-evolution of CO upon lignin/attapulgite pyrolysis, which was

less pronounced for lignin–calcium hydroxide pyrolysis (Fig. 8).

The reaction scheme of the pyrolysis of lignin/attapulgite is presented in Fig. 14. The first conversions for lignin/attapulgite are primary reactions and are the same as those for pure organosolv lignin pyrolysis (indicated by the dark-blue color). First, lignin (exemplified by a lignin dimer) undergoes dehydration followed by its β-O-4 homolytic cleavage, resulting in a *p*-quinone methide radical. This *p*-quinone methide radical is partially stabilised with resonance. In the absence of the clay matrix, (*i.e.*, for pure lignin pyrolysis) 4-(3-hydroxy-1-propenyl)-2-methoxyphenol was found in the pyrolysis vapors, which was identified as the determining compound using pure lignin analytical pyrolysis (Fig. 4b); its relative peak area was 0.83% for pure lignin, while it was 0.23% for lignin/attapulgite (Table 1 in ESI†). While 4-(3-hydroxy-1-propenyl)-2-methoxyphenol can consecutively react to *e.g.*, catechols (Table 3) in secondary reactions, the addition of attapulgite also leads to secondary reactions (orange-colored steps), ultimately leading to 2-propenal, phenol, CO, and methylphenol. This was motivated by a combination of (i) increased cracking opportunities of the 4-(3-hydroxy-1-propenyl)-2-methoxyphenol radical due to the increased retention in the attapulgite porous matrix; and (ii) the steric interaction (stabilization/protection) of that radical with the surrounding clay. The increased retention was hypothesized from the observed porous matrix, left after burning off lignin from lignin/clay (Fig. 2 in ESI†). Steric radical stabilization/protection was put forth, based on the radical trapping/stabilization observed for attapulgite[69,70] and zeolite.[71,72] The consecutive cracking of the 2-methoxyphenol radical into phenol and methylphenol was based on experimental and modelling studies summarized by Kawamoto.[73]

3.8.2. Lignin–calcium hydroxide. From the absence of an endothermic $Ca(OH)_2$ degradation peak in TGA/DSC analysis, it was clear that no free calcium hydroxide was present in the lignin–calcium hydroxide mixture. In the current mechanism from the literature, the phenolic hydroxyl group in lignin bonds to calcium hydroxide as a mono salt.[52] This was based on the observations of Schlosberg and Scouten[56] that $Ca(OH)_2$ reacts with ϕ-OH to form ϕ-O–CaOH. However, the results of the studies by Zhou *et al.*[52] and Li *et al.*[54] cannot exclude the formation of a cross-linked structure, like lignin–O–Ca–O–ϕ–lignin. Instead, the FT-IR spectra of lignin–calcium hydroxide recorded by Zhou *et al.*[52] and Li *et al.*[54] and the FT-IR spectra for various pure (methoxy)phenols precipitated with calcium hydroxide recorded by Schlosberg and Scouten[56] and Hao *et al.*[74] seem to support the hypothesis that two lignin–phenolic moieties react with calcium hydroxide and thus induce cross-linking.

In the FT-IR spectrum of pure calcium hydroxide in hydroxycalcium phenoxide (ϕ-O–CaOH), a sharp peak for OH stretching was apparent at ν = 3640 cm^{-1}.[52,56] This peak was, however, not observed in the FT-IR spectra for lignin to which calcium hydroxide was added.[52,54] The addition of calcium hydroxide to pure methoxyphenols (guaiacol, syringol, 4-ethylguaiacol, and acetosyringone), phenol, and 4-ethylphenol by Hao *et al.*[74] led to a precipitate in case of the methoxyphenols, but not for phenol and 4-ethylphenol. Those precipitates also lacked a characteristic peak for OH at ν = 3640 cm^{-1}, which would be apparent if half salts would have been formed. So, while phenol indeed forms hydroxycalcium phenoxide, it is likely that lignin (and individual methoxyphenols) formed calcium di-salts.

During the pyrolysis of lignin–calcium hydroxide, the following typical compounds increased: methylphenols (Fig. 5b and 10), phenol (Fig. 10), naphthalene (Fig. 10 and 13), methanol (Table 2 in ESI†), C3 compounds (1-hydroxy-2-propanone, 2-propenal, Fig. 4b), and hydrogen gas (Fig. 8). The heavy phase also was most deoxygenated and showed the lowest H/C ratio (Table 2). Fig. 14 exemplifies a reaction mechanism that could explain the formation of the abovementioned compounds.

It starts with the above-hypothesized calcium-induced cross-linked lignin structure that upon thermohydrolysis (heterolytic) or homolytic cleavage, results in a lignin oligomer with its phenolic moiety bound to calcium hydroxide. Consecutive homolytic cleavage of the β-O-4 bond, rearrangement, and keto–enol tautomerism leads to a 1-hydroxy-3-(4-hydroxy-3-methoxyphenyl)propan-2-one of which the phenolic OH was bound to calcium hydroxide. From that point, 1-hydroxy-2-propanone can homolytically be released, resulting in phenol, methanol, and calcium oxide in one route and 2-methylphenol and calcium oxide in the other route. The scheme in Fig. 14 also shows that various phenolics, including phenol and 2-methylphenol, can undergo further aromatic condensation to form naphthalene and other polyaromatic hydrocarbons, catalysed by calcium oxide and associated with the release of hydrogen gas. This formation of naphthalene and hydrogen gas in the presence of calcium oxide has not been pointed out by previous studies[51,52,54] with lignin–calcium hydroxide pyrolysis, but is supported by other studies.[75–78] As sand and the formed calcium oxide were retained in the reactor, calcium oxide could engage in catalytic condensation reactions with the gaseous intermediates.

3.8.3. Lignin/sodium formate. The presence of 2-methoxyphenol and 2,6-dimethoxyphenol in the pyrograms and heavy pyrolysis liquids was very characteristic of pyrolysis of lignin/sodium formate. A reaction scheme as shown in Fig. 14 is put forth which shows how methoxyphenols can be formed, along with the co-evolution of H_2 and CO. As observed from analytical pyrolysis (Table 1 in ESI†), and consistent with Ref. 48, more saturated side-chains of (methoxy)phenols were present, like 4-(3-hydroxypropyl)-2-methoxyphenol or dihydroconyferyl alcohol. All these were due to the formation of atomic hydrogen upon sodium formate decomposition. This atomic hydrogen can undergo self-quenching to form H_2, induce the homolytic C–C and C–O cleavage, and quench the radical intermediates to form *e.g.*, stable methoxyphenols found in the liquids.[48] During secondary reactions upon reactor-scale pyrolysis, these side chains are converted into light compounds, resulting in methoxyphenols (Fig. 10 and 12).

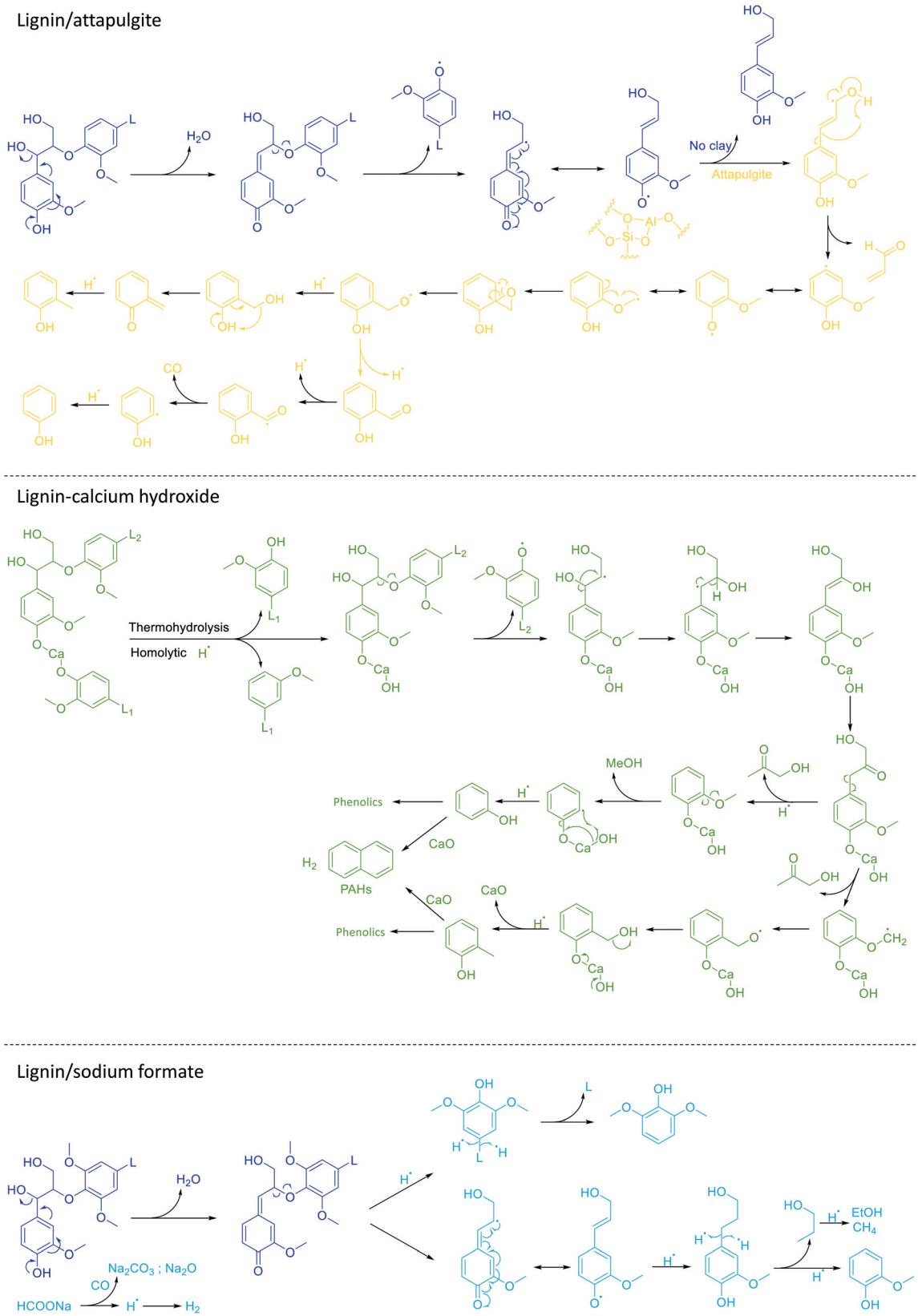

Fig. 14 Putative, non-stoichiometric reaction scheme of lignin/attapulgite (top), lignin–calcium hydroxide (middle), and lignin/sodium formate (bottom). Dark-blue compounds result from the primary reactions of lignin that occur along with reactions specific to lignin with a certain additive (orange, green, and light-blue).

4. Conclusions

This work compared three different lignin additives, clay, calcium hydroxide, and sodium formate, and evaluated their effects on the production of liquids rich in monoaromatic compounds by analytical and reactor-scale pyrolysis in a well-defined manner. First, every additive did significantly improve reactor introduction by hindering lignin's mobility, either physically (in case of attapulgite clay and sodium formate addition) or by cross-linkages of the different lignin fragments (in case of calcium hydroxide addition). The liquid yield increased from *ca.* 11 wt% for pure lignin to 23–47 wt% for all lignins with additives.

Lignin/attapulgite was shown as one of the most promising and simple additives. Indeed, the heavy phase from lignin/attapulgite provided the highest carbon yield (25.7%), a substantial monomer yield (18.9% on liquid basis), and the highest absolute yield of cresylic acids (phenol, cresols, and xylenols) being 1.34 wt% on lignin basis. Pyrolysis of lignin–calcium hydroxide yielded the highest monomer yield (23.8% on liquid basis) in the heavy phase, with a substantial carbon yield (15.1%). The addition of calcium hydroxide was the second-best for cresylic acid production. For methoxylated benzene/phenol production, the addition of sodium formate was best among the additives, but the rather low carbon and mass yield of the heavy phase resulted in a modest absolute yield of 0.46 wt% on lignin basis.

Regarding the pyrolysis mechanisms, it was shown that the addition of attapulgite induced small changes in the compound portfolio, possibly due to more cracking opportunities from the longer vapor residence time in the attapulgite matrix and attapulgite-induced radical stabilization. For pyrolysis of lignin with calcium hydroxide, it has been put forth that calcium could bind to two lignin–OH moieties and that calcium oxide is formed which can catalyze the formation of naphthalene and polyaromatic compounds. Pyrolysis of lignin/sodium formate resulted in the least quantity of dimeric compounds and the highest fraction of methoxyphenols in the heavy phase, which is attributed to the released hydrogen atoms that can quench the reactive radical intermediates.

Overall, this work (i) shows that attapulgite and calcium hydroxide especially hold value as additives towards monoaromatic compounds (like cresylic acid) and (ii) sheds new light on the molecular-scale pyrolysis mechanisms of lignin with and without additives.

Conflicts of interest

There are no conflicts to declare.

Acknowledgements

This study received funding from the European Union's Horizon 2020 research and innovation programme under the Marie Sklodowska-Curie grant agreement no. 721991. Fraunhofer is particularly acknowledged for the production of organosolv lignin. Tolsa is acknowledged for providing the clay materials.

References

1 F. Calvo-Flores, J. Dobado, J. Isac-García and F. Martín-MartíNez, in *Background and Overview*, John Wiley & Sons, Ltd, 2015, ch. 1, pp. 1–8.
2 F. Calvo-Flores, J. Dobado, J. Isac-García and F. Martín-MartíNez, in *Structure and Physicochemical Properties*, John Wiley & Sons, Ltd, 2015, ch. 2, pp. 9–48.
3 W. Fang, S. Yang, X.-L. Wang, T.-Q. Yuan and R.-C. Sun, *Green Chem.*, 2017, **19**, 1794–1827.
4 H. Liu, Z. Dai, Q. Cao, X. Shi, X. Wang, H. Li, Y. Han, Y. Li and J. Zhou, *ACS Sustainable Chem. Eng.*, 2018, **6**, 8554–8562.
5 D.-W. Lee, M.-H. Jin, J.-H. Park, Y.-J. Lee and Y.-C. Choi, *ACS Sustainable Chem. Eng.*, 2018, **6**, 10454–10462.
6 M. Graglia, J. Pampel, T. Hantke, T.-P. Fellinger and D. Esposito, *ACS Nano*, 2016, **10**, 4364–4371.
7 S. Ghysels, F. Ronsse, D. Dickinson and W. Prins, *Biomass Bioenergy*, 2019, **122**, 349–360.
8 B. M. Upton and A. M. Kasko, *Chem. Soc. Rev.*, 2016, **116**, 2275–2306.
9 D. Barana, M. Orlandi, L. Zoia, L. Castellani, T. Hanel, C. Bolck and R. Gosselink, *ACS Sustainable Chem. Eng.*, 2018, **6**, 11843–11852.
10 W. Liu, R. Zhou, H. L. S. Goh, S. Huang and X. Lu, *ACS Appl. Mater. Interfaces*, 2014, **6**, 5810–5817.
11 Y. Zhang, S. Zhou, X. Fang, X. Zhou, J. Wang, F. Bai and S. Peng, *Eur. Polym. J.*, 2019, **116**, 265–274.
12 J. Gao, H. Wang, C. Liu, D. Ge, Z. You and M. Yu, *Constr. Build. Mater.*, 2020, **230**, 117063.
13 C. Li, X. Zhao, A. Wang, G. W. Huber and T. Zhang, *Chem. Soc. Rev.*, 2015, **115**, 11559–11624.
14 M. P. Pandey and C. S. Kim, *Chem. Eng. Technol.*, 2011, **34**, 29–41.
15 R. Rinaldi, R. Jastrzebski, M. T. Clough, J. Ralph, M. Kennema, P. C. A. Bruijnincx and B. M. Weckhuysen, *Angew. Chem., Int. Ed.*, 2016, **55**, 8164–8215.
16 S. Van den Bosch, S.-F. Koelewijn, T. Renders, G. Van den Bossche, T. Vangeel, W. Schutyser and B. F. Sels, *Top. Curr. Chem.*, 2018, **376**, 36.
17 Z. Sun, B. Fridrich, A. de Santi, S. Elangovan and K. Barta, *Chem. Soc. Rev.*, 2018, **118**, 614–678.
18 C. Xu, R. A. D. Arancon, J. Labidi and R. Luque, *Chem. Soc. Rev.*, 2014, **43**, 7485–7500.
19 R. Venderbosch and W. Prins, *Biofuels, Bioprod. Biorefin.*, 2010, **4**, 178–208.
20 L. Fan, Y. Zhang, S. Liu, N. Zhou, P. Chen, Y. Cheng, M. Addy, Q. Lu, M. M. Omar, Y. Liu, Y. Wang, L. Dai, E. Anderson, P. Peng, H. Lei and R. Ruan, *Bioresour. Technol.*, 2017, **241**, 1118–1126.

21 X. Bai, K. H. Kim, R. C. Brown, E. Dalluge, C. Hutchinson, Y. J. Lee and D. Dalluge, *Fuel*, 2014, **128**, 170–179.
22 S. Jampa, A. Puente-Urbina, Z. Ma, S. Wongkasemjit, J. S. Luterbacher and J. A. van Bokhoven, *ACS Sustainable Chem. Eng.*, 2019, **7**, 4058–4068.
23 M. Windt, D. Meier, J. H. Marsman, H. J. Heeres and S. de Koning, *J. Anal. Appl. Pyrolysis*, 2009, **85**, 38–46.
24 M. Lei, S. Wu, J. Liang and C. Liu, *J. Anal. Appl. Pyrolysis*, 2019, **138**, 249–260.
25 P. R. Patwardhan, D. L. Dalluge, B. H. Shanks and R. C. Brown, *Bioresour. Technol.*, 2011, **102**, 5265–5269.
26 M. Ringer, V. Putsche and J. Scahill, Large-Scale Pyrolysis Oil Production: A Technology Assessment and Economic Analysis, National Renewable Energy Laboratoy (NREL) technical report, 2016.
27 D. Nowakowski, A. Bridgwater, D. Elliott, D. Meier and P. de Wild, *J. Anal. Appl. Pyrolysis*, 2010, **88**, 53–72.
28 F. Berruti, L. Ferrante, F. Berruti and C. Briens, *Int. J. Chem. React. Eng.*, 2009, **7**, A84.
29 D. Li, C. Briens and F. Berruti, *Bioresour. Technol.*, 2015, **189**, 7–14.
30 T. Han, N. Sophonrat, A. Tagami, O. Sevastyanova, P. Mellin and W. Yang, *Fuel*, 2019, **235**, 1061–1069.
31 B. Shrestha, Y. le Brech, T. Ghislain, S. Leclerc, V. Carré, F. Aubriet, S. Hoppe, P. Marchal, S. Pontvianne, N. Brosse and A. Dufour, *ACS Sustainable Chem. Eng.*, 2017, **5**, 6940–6949.
32 D. Howe, M. Garcia-Perez, D. Taasevigen, J. Rainbolt, K. Albrecht, H. Li, L. Wei, A. McDonald and M. Wolcott, *J. Anal. Appl. Pyrolysis*, 2019, **142**, 103691.
33 S. Zhou, B. Pecha, M. van Kuppevelt, A. G. McDonald and M. Garcia-Perez, *Biomass Bioenergy*, 2014, **66**, 398–409.
34 H. Cheng, S. Wu, J. Huang and X. Zhang, *Anal. Bioanal. Chem.*, 2017, **409**, 2531–2537.
35 K. H. Kim, T. Dutta, E. D. Walter, N. G. Isern, J. R. Cort, B. A. Simmons and S. Singh, *ACS Sustainable Chem. Eng.*, 2017, **5**, 3913–3919.
36 C. Bährle, V. Custodis, G. Jeschke, J. Van Bokhoven and F. Vogel, *ChemSusChem*, 2014, **7**, 2022–2029.
37 S. Chu, A. V. Subrahmanyam and G. W. Huber, *Green Chem.*, 2013, **15**, 125–136.
38 Q. Sun, R. Khunsupat, K. Akato, J. Tao, N. Labbé, N. C. Gallego, J. J. Bozell, T. G. Rials, G. A. Tuskan, T. J. Tschaplinski, A. K. Naskar, Y. Pu and A. J. Ragauskas, *Green Chem.*, 2016, **18**, 5015–5024.
39 P. Sirous-Rezaei and Y.-K. Park, *Chem. Eng. J.*, 2019, 121348.
40 T. L. Marker, L. G. Felix, M. B. Linck and M. J. Roberts, *Environ. Prog. Sustainable Energy*, 2012, **31**, 191–199.
41 O. Jan, R. Marchand, L. C. A. Anjos, G. V. S. Seufitelli, E. Nikolla and F. L. P. Resende, *Energy Fuels*, 2015, **29**, 1793–1800.
42 A. Kloekhorst and H. J. Heeres, *ACS Sustainable Chem. Eng.*, 2015, **3**, 1905–1914.
43 A. Kloekhorst, J. Wildschut and H. J. Heeres, *Catal. Sci. Technol.*, 2014, **4**, 2367–2377.
44 C. R. Kumar, N. Anand, A. Kloekhorst, C. Cannilla, G. Bonura, F. Frusteri, K. Barta and H. J. Heeres, *Green Chem.*, 2015, **17**, 4921–4930.
45 R. Wilberink, R. Van der Laan and P. de Wild, WO2011159154 - pyrolysis of lignin, 2011.
46 P. de Wild, W. Huijgen, A. Kloekhorst, R. Chowdari and H. Heeres, *Bioresour. Technol.*, 2017, **229**, 160–168.
47 W. Wang, M. Wang, J. Huang, X. Zhao, Y. Su, Y. Wang and X. Li, *Bioresour. Technol.*, 2019, **278**, 464–467.
48 W. Li, S. Zhou, Y. Xue, Y.-J. Lee, R. Smith and X. Bai, *ACS Sustainable Chem. Eng.*, 2017, **5**, 8939–8950.
49 S. Mukkamala, M. C. Wheeler, A. R. P. van Heiningen and W. J. DeSisto, *Energy Fuels*, 2012, **26**, 1380–1384.
50 J. Geng, W.-L. Wang, Y.-X. Yu, J.-M. Chang, L. P. Cai and S. Q. Shi, *Bioresour. Technol.*, 2017, **227**, 1–6.
51 Y. Cui, W. Wang and J. Chang, *Materials*, 2019, **12**, 1609.
52 S. Zhou, R. C. Brown and X. Bai, *Green Chem.*, 2015, **17**, 4748–4759.
53 H. W. Lee, Y.-M. Kim, J. Jae, S. M. Lee, S.-C. Jung and Y.-K. Park, *Renewable Energy*, 2019, **144**, 147–152.
54 J. Li, X. Bai, Z. Dong, Y. Chen, H. Yang, X. Wang and H. Chen, *Fuel*, 2020, **263**, 116629.
55 P. Schulze, A. Seidel-Morgenstern, H. Lorenz, M. Leschinsky and G. Unkelbach, *Bioresour. Technol.*, 2016, **199**, 128–134.
56 R. H. Schlosberg and C. G. Scouten, *Energy Fuels*, 1988, **2**, 582–585.
57 T. Meisel, Z. Halmos, K. Seybold and E. Pungor, *J. Therm. Anal.*, 1975, **7**, 73–80.
58 H. E. Toraman, R. Vanholme, E. Borén, Y. Vanwonterghem, M. R. Djokic, G. Yildiz, F. Ronsse, W. Prins, W. Boerjan, K. M. V. Geem and G. B. Marin, *Bioresour. Technol.*, 2016, **207**, 229–236.
59 H. Gao, T. Jiang, M. Zhou, J. Wen, X. Li, Y. Wang and X. Xue, *Miner. Eng.*, 2020, **145**, 106056.
60 J. Montoya, B. Pecha, F. C. Janna and M. Garcia-Perez, *J. Anal. Appl. Pyrolysis*, 2016, **122**, 106–121.
61 F. Calvo-Flores, J. Dobado, J. Isac-García and F. Martín-MartíNez, in *Functional and Spectroscopic Characterization of Lignins*, John Wiley & Sons, Ltd, 2015, ch. 6, pp. 145–188.
62 H. Fiege, in *Cresols and Xylenols*, American Chemical Society, 2000.
63 O. D. Mante, S. J. Thompson, S. Mustapha and D. C. Dayton, *Green Chem.*, 2019, **21**, 2257–2265.
64 N. Mahmood, Z. Yuan, J. Schmidt and C. C. Xu, *Renewable Sustainable Energy Rev.*, 2016, **60**, 317–329.
65 X. Zhao, H. Chen, F. Kong, Y. Zhang, S. Wang, S. Liu, L. A. Lucia, P. Fatehi and H. Pang, *Chem. Eng. J.*, 2019, **364**, 226–243.
66 M. Figueirêdo, Z. Jotic, P. Deuss, R. Venderbosch and H. Heeres, *Fuel Process. Technol.*, 2019, **189**, 28–38.
67 H. Ben and A. Ragauskas, *Energy Fuels*, 2011, **25**, 5791–5801.
68 N. Hao, H. Ben, C. Yoo, S. Adhikari and A. Ragauskas, *Energy Fuels*, 2016, **30**, 6863–6880.

69 F. Yang and G. Nelson, 20th Annual Conference on Recent Advances in Flame Retardancy of Polymeric Materials 2009, 2009, pp. 160–170.
70 J. Zhu, F. M. Uhl, A. B. Morgan and C. A. Wilkie, *Chem. Mater.*, 2001, **13**, 4649–4654.
71 S. Jockusch, T. Hirano, Z. Liu and N. J. Turro, *J. Phys. Chem.*, 2000, **104**, 1212–1216.
72 B. Tang, J. Zhao, J.-F. Xu and X. Zhang, *Chem. Sci.*, 2020, **11**, 1192–1204.
73 H. Kawamoto, *J. Wood Sci.*, 2017, **63**, 117–132.
74 S. Hao, K. Chen, L. Cao, X. Zhu, G. Luo, S. Zhang and J. Chen, *Electrophoresis*, 2016, **37**, 2522–2530.
75 Y.-L. Wei and J.-H. Lee, *Sci. Total Environ.*, 1998, **212**, 173–181.
76 N. Sophonrat, L. Sandström, R. Svanberg, T. Han, S. Dvinskikh, C. M. Lousada and W. Yang, *Ind. Eng. Chem. Res.*, 2019, **58**, 13960–13970.
77 Y. Lin, C. Zhang, M. Zhang and J. Zhang, *Energy Fuels*, 2010, **24**, 5686–5695.
78 L. Zhang, B. Zhang, Z. Yang and Y. Yan, *RSC Adv.*, 2014, **4**, 39145–39155.